IEEE Access
Multidisciplinary | Rapid Review | Open Access Journal

Received August 30, 2021, accepted September 29, 2021, date of publication October 4, 2021, date of current version October 12, 2021.

Digital Object Identifier 10.1109/ACCESS.2021.3117704

Design and Verification of Attitude Control System for a Boost-Glide Rocket

XIAOSHUAI FAN, XIBIN BAI, ZHENYU JIANG, LONGBIN LIU, AND SHIFENG ZHANG
College of Aerospace Science and Engineering, National University of Defense Technology, Changsha 410073, China

Corresponding author: Longbin Liu (longbuaa@163.com)

This work was supported in part by the National Natural Science Foundation of China under Grant 11802334.

ABSTRACT The boost-glide rocket needs to maneuver in the atmosphere with complex flight conditions, which is a big challenge for the attitude control system. In this paper, the design process of the control system is analyzed. With specific points of the flight trajectory, the design of an improved proportional-integrative-derivative (PID) controller based on the small perturbation theory is carried out. Design approach of the attitude control system is verified by the six-degree-freedom model simulation. The rocket flight control program is written to the onboard computer so that hardware-in-the-loop simulation experiment is completed. Experimental results show that the mean and standard deviation of the error between simulation value and experiment value are below 0.5°, so the control parameters and design method are reasonable with a great attitude tracking effect. This paper proposes the design and verification method of a boost-glide rocket attitude control system, which can provide a reference for design of the boost-glide rocket around the world.

INDEX TERMS Boost-glide, attitude control, PID, hardware-in-the-loop simulation.

I. INTRODUCTION

Boost-glide rocket is the hotspot object of current research, which can maneuver in the atmosphere to complete specific flight missions. It can achieve great success with the joint execution of multiple rockets [1], [2]. The boost-glide rocket has many advantages such as high speed, long-range, and high accuracy. Design and application of the control system is a big challenge for high maneuver flight. The boost-glide rocket changes attitude by rudder deflection, which requires fast-tracking ability of the command attitude angle. It could hit the target and complete missions by correcting attitude deviation constantly.

The boost-glide rocket obtains guidance instructions from measurement data of sensors, then generates control torque to change the angular velocity and attitude angle. The attitude control system is a complex mechatronics system, which not only needs to ensure correctness of the calculation algorithm but also needs to ensure normal work of the flight control program and reliability of the hardware. The control system is composed of a variety of software and hardware, any problem in the loop will lead to failure of the whole mission [3]. However, the rocket is in a bad flight environment for a long time, disturbance and complex electromagnetic environment will lead to failure frequently, the control chip's voltage inversion caused by disturbance will make the control process generate errors and result in serious flight accidents.

The attitude control system is basis for a boost-glide rocket to complete flight missions. Attitude divergence is a high-frequency problem of rockets, which is also the focus of research by scholars in related fields [4]–[9]. Common control methods include adaptive control [10]–[12], control allocation [13]–[15], sliding mode control [16]–[18], multi-model switching control [19]–[21], nonlinear control, etc. [22]. The design of a controller with stability and strong robustness is the focus of current research. Wei *et al.* [23] propose a formation keeping controller. In [24], Wei *et al.* design an adaptive control controller. In [25], Wang *et al.* propose a method to deal with tracking and attitude control problems. However, most of the current advances only remain at the theoretical level with pure numerical simulation, lack of experimental verification, so it is difficult to obtain engineering applications.

Taking a small boost-glide rocket as an example shown in Fig. 1, we will analyze the control system working principle and hardware composition, propose the transfer function

The associate editor coordinating the review of this manuscript and approving it for publication was Haibin Sun.

FIGURE 1. A physical view of the propulsion glide technology test aircraft.

calculation method and the control law design method. The three-channel control law will be designed and verified through nonlinear six-degree-freedom trajectory simulation and hardware-in-the-loop simulation experiment. The experimental results have high reliability and universality, which can provide a reference for design of an attitude control system with the boost-glide aircraft.

II. DESIGN OF THE ATTITUDE CONTROL SYSTEM

A. OVERALL CONCEPT DESIGN

There are three parts of the overall concept design.

1) COMPOSITION OF THE ATTITUDE CONTROL SYSTEM

Block diagram of the attitude control system is shown in Fig. 2. While the rocket is flying in the atmosphere, it is affected by various disturbances, which cause the actual attitude angle to deviate from the command attitude angle. The actual attitude angle is calculated by the integrated navigation system. The attitude controller calculates rudder deflection instruction according to attitude deviation and transfers it to the rudder system to have deflection angle, then it will generate control torque to change attitude of the rocket.

Components of the attitude control system are shown in Fig. 3.

Simulation is required for a control system of the boost-glide rocket. Flight process of the rocket is simulated by Real-Time Model Solution Platform, integrated navigation, flight control computer, and rudder controller, which are integrated into integrated flight control machine, as shown in Fig. 4.

2) BLOCK DIAGRAM SIMPLIFICATION

When designing the control law, it is considered that there is no disturbance and the measuring sensor and actuator are ideal equipment. Block diagram of the control law is simplified as shown in Fig. 5.

3) DESIGN PROCESS OF THE BOOST-GLIDE ROCKET ATTITUDE CONTROL LAW

First, we should calculate three-channel transfer function of the boost-glide rocket, then derive transfer function of the control system. Finally, adjusting control parameters to make performance of the control system meet requirements of indicators, the process is shown in Fig. 6.

B. ROCKET THREE-CHANNEL TRANSFER FUNCTION

There are five steps to get the rocket three-channel transfer function.

1) MOVEMENT MODEL

Movement model of the rocket is established, specific symbol meaning is referred to [26]. The model is divided into longitudinal movement model and lateral movement model. Variables of the longitudinal model include velocity, velocity inclination angle, attack angle, pitch angle, pitch angular velocity, transmitting orientation displacement and altitude, etc., which can be expressed as

$$\begin{cases} m\dfrac{dV}{dt} = P\cos\alpha\cos\beta - X - mg\sin\theta\cos\sigma + F_{cxv1} \\ mV\dfrac{d\theta}{dt}\cos\sigma \\ = P(\sin\alpha\cos\nu + \cos\alpha\sin\beta\sin\nu) \\ \quad +Y\cos\nu - Z\sin\nu - mg\cos\theta + R'\delta_\varphi\cos\nu \\ \quad +R'\delta_\psi\sin\nu \\ I_{z1}\dot{\omega}_{z1} = M_{z1} + M_{z1}^{\delta}\delta_\varphi + (I_{x1} - I_{y1})\omega_{x1}\omega_{y1} \\ \dfrac{dx}{dt} = V\cos\theta\cos\sigma \\ \dfrac{dy}{dt} = V\sin\theta\cos\sigma \\ \omega_{z1} = \dot{\varphi}\cos\psi\cos\gamma - \dot{\psi}\sin\gamma \\ \varphi = \theta + \alpha \end{cases} \tag{1}$$

Variables of the lateral motion model include track yaw angle, sideslip angle, yaw angle, yaw angular velocity, roll angle, roll angular velocity, and lateral distance, etc., which can be expressed as

$$\begin{cases} -mV\dfrac{d\sigma}{dt} \\ = P(\sin\alpha\sin\nu - \cos\alpha\sin\beta\cos\nu) \\ +Y\sin\nu + Z\cos\nu - mg\sin\theta\sin\sigma \\ \quad +R'\delta_\varphi\sin\nu - R'\delta_\psi\cos\nu \\ I_{x1}\dot{\omega}_{x1} = M_{x1} + M_{x1}^{\delta}\delta_\gamma + (I_{y1} - I_{z1})\omega_{y1}\omega_{z1} \\ I_{y1}\dot{\omega}_{y1} = M_{y1} + M_{y1}^{\delta}\delta_\psi + (I_{z1} - I_{x1})\omega_{z1}\omega_{x1} \\ \dfrac{dz}{dt} = -V\sin\sigma \\ \omega_{x1} = \dot{\gamma} - \dot{\varphi}\sin\psi \\ \omega_{y1} = \dot{\psi}\cos\gamma + \dot{\varphi}\cos\psi\sin\gamma \\ \psi = \sigma + \beta \\ \gamma = \nu \end{cases} \tag{2}$$

2) LINEARIZATION OF THE BOOST-GLIDE ROCKET MOVEMENT MODEL

Longitudinal and lateral motion models of the rocket are nonlinear, parameter time-varying with modeling errors,

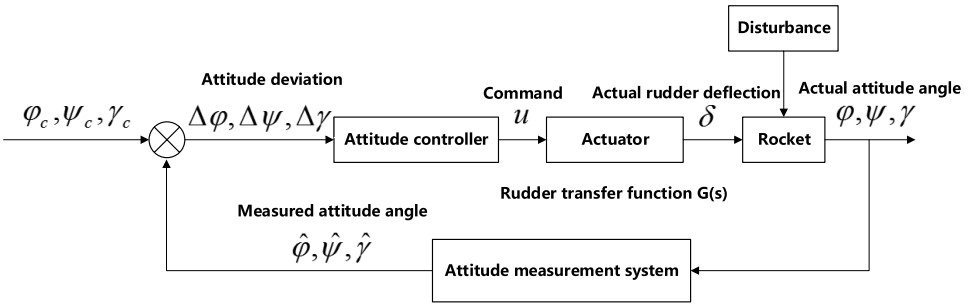

FIGURE 2. Block diagram of the attitude control system.

(a) Body of the boost-glide rocket

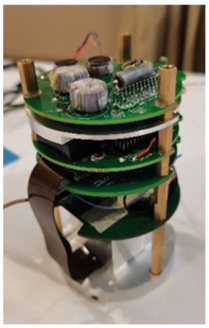

(b) Integrated navigation and rudder controller

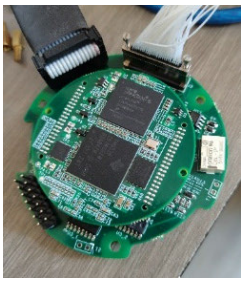

(c) Flight control computer

(d) The rudder system

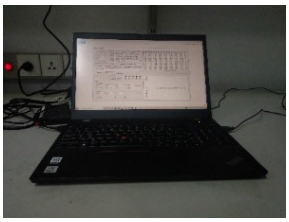

(e) Ground station

(f) Telemetry hardware

FIGURE 3. Components of the control system for a boost-glide rocket.

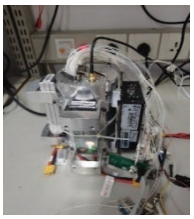

(a) Integrated flight control machine

(b) Real-Time Model Solution Platform

FIGURE 4. Simulation equipment of the attitude control system.

so models need to be linearized to facilitate the derivation of the transfer function. The perturbation equation of a

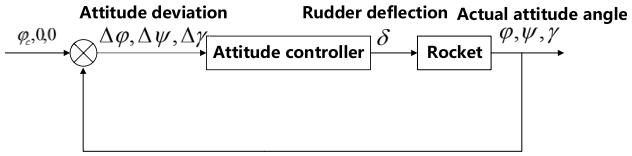

FIGURE 5. Simplified block diagram of the attitude control law.

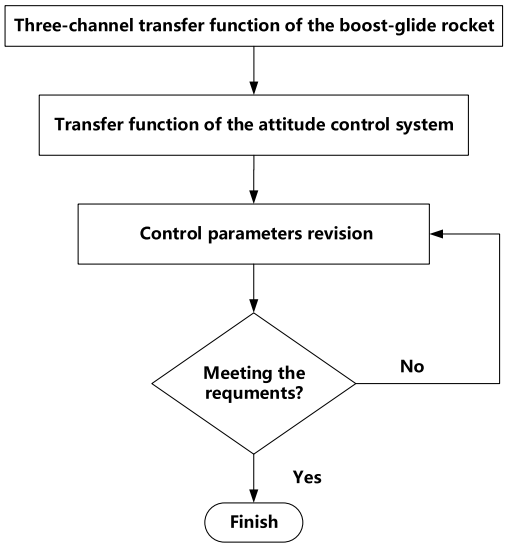

FIGURE 6. Design process of the boost-glide rocket attitude control law.

rocket is derived by small perturbation method on theoretical trajectory.

The longitudinal perturbation model is expressed as

$$\begin{cases} m\dfrac{\mathrm{d}V}{\mathrm{d}t} = \left(P^V\cos\alpha - X^V\right)\mathrm{d}V - (P\sin\alpha + X^\alpha)\mathrm{d}\alpha \\ \qquad\qquad -mg\cos\theta\mathrm{d}\theta \\ mV\dfrac{\mathrm{d}\theta}{\mathrm{d}t} = \left(P^V\sin\alpha + Y^V - m\dfrac{\mathrm{d}\theta}{\mathrm{d}t}\right)\mathrm{d}V \\ \qquad\qquad + \left(P\cos\alpha + Y^\alpha\right)\mathrm{d}\alpha + mg\sin\theta\mathrm{d}\theta + Y^{\delta_\varphi}\mathrm{d}\delta_\varphi \\ I_{z1}\dfrac{\mathrm{d}\omega_{z1}}{dt} = M_{z1}^V\mathrm{d}V + M_{z1}^\alpha\mathrm{d}\alpha + M_{z1}^{\omega_z}\mathrm{d}\omega_z \\ \qquad\qquad + M_{z1}^\delta\mathrm{d}\delta_\varphi + M_{zB} \\ \mathrm{d}\varphi = \mathrm{d}\theta + \mathrm{d}\alpha \\ \omega_{z1} = \dfrac{\mathrm{d}\varphi}{\mathrm{d}t} \\ \dfrac{\mathrm{d}x}{\mathrm{d}t} = \cos\theta V - V\sin\theta\Delta\theta \\ \Delta\dot{y} = \sin\theta\Delta V + V\cos\theta\Delta\theta \end{cases} \tag{3}$$

The longitudinal perturbation model is also expressed as

$$\begin{cases} \dfrac{d\Delta V}{dt} = a_{11}\Delta V + a_{12}\Delta\theta + a_{13}\Delta\alpha \\ \dfrac{d\Delta\theta}{dt} = a_{21}\Delta V + a_{22}\Delta\theta + a_{23}\Delta\alpha + a_{25}\Delta\delta_\varphi \\ \dfrac{d\Delta\alpha}{dt} = a_{31}\Delta V + a_{32}\Delta\theta + a_{33}\Delta\alpha + a_{34}\Delta\omega_{z1} \\ \qquad\qquad +a_{35}\Delta\delta_\varphi \\ \dfrac{d\Delta\omega_{z1}}{dt} = a_{41}\Delta V + a_{42}\Delta\theta + a_{43}\Delta\alpha + a_{44}\Delta\omega_{z1} \\ \qquad\qquad +a_{45}\Delta\delta_\varphi \end{cases} \tag{4}$$

where

$$\begin{aligned} a_{11} &= \frac{P^V\cos\alpha - X^V}{m}, \quad a_{12} = -g\cos\theta, \\ a_{13} &= \frac{-P\sin\alpha - X^\alpha}{m}, \quad a_{14} = 0, \\ a_{21} &= \frac{P^V\sin\alpha + Y^V - m\dot\theta}{mV}, \quad a_{22} = \frac{g\sin\theta}{V}, \\ a_{23} &= \frac{P\cos\alpha + Y^\alpha}{mV}, \quad a_{24} = 0, \quad a_{25} = \frac{Y^{\delta_\varphi}}{mV}, \\ a_{31} &= -a_{21} = -\frac{\left(P^V\sin\alpha + Y^V - m\dot\theta\right)}{mV}, \\ a_{32} &= -a_{22} = -\frac{g\sin\theta}{V}, \quad a_{33} = -a_{23} = -\frac{P\cos\alpha + Y^\alpha}{mV}, \\ a_{34} &= 1, a_{35} = -\frac{Y^{\delta_\theta}}{mV}, \quad a_{41} = \frac{M_{z1}^V}{I_{z1}}, a_{43} = \frac{M_{z1}^\alpha}{I_{z1}}, \\ a_{44} &= \frac{M_{z1}^{\omega_z}}{I_{z1}}, \quad a_{45} = \frac{M_{z1}^\delta}{I_{z1}} \end{aligned} \tag{5}$$

The lateral perturbation model is expressed as

$$\begin{cases} -mV\dfrac{d\Delta\sigma}{dt} \\ = \left(-P\cos\alpha\cos\beta + Z^\beta\right)\Delta\beta - mg\sin\theta\Delta\sigma \\ + \left(P\sin\alpha + Y\right)\Delta\nu - Z^{\delta_\psi}\cos\nu\Delta\delta_\psi + F_{dz} \\ I_{x1}\dfrac{d\Delta\omega_{x1}}{dt} = M_{x1}^\beta\Delta\beta + M_{x1}^{\omega_{x1}}\Delta\omega_x + M_{x1}^{\omega_{y1}}\Delta\omega_y \\ \qquad\qquad +M_{x1}^{\delta_\gamma}\Delta\delta_\gamma + M_{xB} \\ I_{y1}\dfrac{d\Delta\omega_{y1}}{dt} = M_{y1}^\beta\Delta\beta + M_{y1}^{\omega_{x1}}\Delta\omega_x + M_{y1}^{\omega_{y1}}\Delta\omega_y \\ \qquad\qquad +M_{y1}^{\delta_\psi}\Delta\delta_\psi + M_{YB} \\ \Delta\omega_{x1} = \Delta\dot\gamma - \dot\varphi\Delta\psi \\ \Delta\omega_{y1} = \Delta\dot\psi + \dot\varphi\Delta\gamma \\ \Delta\sigma = \Delta\psi - \Delta\beta \\ \Delta\nu = \Delta\gamma \\ \Delta\dot z = -V\Delta\sigma \end{cases} \tag{6}$$

The lateral perturbation model is also expressed as

$$\begin{cases} \dfrac{d\Delta\beta}{dt} = -b_{11}\Delta\beta - b_{12}\Delta\psi - b_{13}\Delta\omega_y - b_{14}\Delta\gamma \\ \qquad\qquad -b_{16}\Delta\delta_\psi \\ \dfrac{d\Delta\psi}{dt} = b_{23}\Delta\omega_{y1} \\ \dfrac{d\Delta\omega_{y1}}{dt} = b_{31}\Delta\beta + b_{33}\Delta\omega_{y1} + b_{35}\Delta\omega_{x1} + b_{36}\Delta\delta_\psi \\ \dfrac{d\Delta\gamma}{dt} = b_{45}\Delta\omega_{x1} \\ \dfrac{d\Delta\omega_{x1}}{dt} = b_{51}\Delta\beta + b_{53}\Delta\omega_{y1} + b_{55}\Delta\omega_{x1} + b_{57}\Delta\delta_\gamma \end{cases} \tag{7}$$

where

$$\begin{aligned} b_{11} &= -\frac{\left(-P\cos\alpha\cos\beta + Z^\beta + mg\sin\theta\right)}{mV}, \; b_{12} = \frac{g\sin\theta}{V}, \\ b_{13} &= -1, \; b_{14} = -\frac{P\sin\alpha + Y}{mV}, b_{15} = 0, \; b_{16} = \frac{Z^{\delta_\psi}}{mV}, \\ b_{23} &= 1, \\ b_{31} &= \frac{M_{y1}^\beta}{I_{y1}}, \; b_{33} = \frac{M_{y1}^{\omega_{y1}}}{I_{y1}}, \; b_{35} = \frac{M_{y1}^{\omega_{x1}}}{I_{y1}}, \; b_{36} = \frac{M_{y1}^{\delta_\psi}}{I_{y1}}, \\ b_{45} &= 1, \\ b_{51} &= \frac{M_{x1}^\beta}{I_{x1}}, \; b_{53} = \frac{M_{x1}^{\omega_{y1}}}{I_{x1}}, \; b_{55} = \frac{M_{x1}^{\omega_{x1}}}{I_{x1}}, \; b_{57} = \frac{M_{x1}^{\delta_\gamma}}{I_{x1}} \end{aligned} \tag{8}$$

The variable calculation method of an aerodynamic derivative is as follows

$$\begin{cases} Y^\alpha = C_{y1}^\alpha\cdot q\cdot S_m \\ Y^{\delta_\varphi} = C_{y1}^{\delta_\varphi}\cdot q\cdot S_m \\ M_{z1}^\alpha = C_{M_{z1}}^\alpha\cdot q\cdot S_m\cdot L_k + Y^\alpha\cdot X_{cg} \\ \qquad = C_{M_{z1}}^\alpha\cdot q\cdot S_m\cdot L_k + C_{y1}^\alpha\cdot q\cdot S_m\cdot X_{cg} \\ M_{z1}^{\delta_\varphi} = C_{M_{z1}}^{\delta_\varphi}\cdot q\cdot S_m\cdot L_k + Y^{\delta_\varphi}\cdot X_{cg} \\ \qquad = C_{M_{z1}}^{\delta_\varphi}\cdot q\cdot S_m\cdot L_k + C_{y1}^{\delta_\varphi}\cdot q\cdot S_m\cdot X_{cg} \\ M_{z1}^{\omega_z} = C_{M_{z1}}^{\omega_z}\cdot q\cdot S_m\cdot L_k\cdot\dfrac{L_k}{V} \\ Z^\beta = C_{z1}^\beta\cdot q\cdot S_m \\ Z^{\delta_\psi} = C_{z1}^{\delta_\psi}\cdot q\cdot S_m \\ M_{y1}^\beta = C_{M_{y1}}^\beta\cdot q\cdot S_m\cdot L_k - Z^\beta\cdot X_{cg} \\ \qquad = C_{M_{y1}}^\beta\cdot q\cdot S_m\cdot L_k - C_{z1}^\beta\cdot q\cdot S_m\cdot X_{cg} \\ M_{y1}^{\delta_\psi} = C_{M_{y1}}^{\delta_\psi}\cdot q\cdot S_m\cdot L_k - Z^\beta\cdot X_{cg} \\ \qquad = C_{M_{y1}}^{\delta_\psi}\cdot q\cdot S_m\cdot L_k - C_{z1}^{\delta_\psi}\cdot q\cdot S_m\cdot X_{cg} \\ M_{y1}^{\omega_{y1}} = C_{M_{y1}}^{\omega_{y1}}\cdot q\cdot S_m\cdot L_k\cdot\dfrac{L_k}{V} \\ M_{x1}^{\omega_{x1}} = C_{M_{x1}}^{\omega_{x1}}\cdot q\cdot S_m\cdot L_k\cdot\dfrac{L_k}{V} \\ M_{x1}^{\delta_\gamma} = C_{M_{x1}}^{\delta_\gamma}\cdot q\cdot S_m\cdot L_k\cdot\dfrac{L_k}{V} \end{cases} \tag{9}$$

where L_k represents the characteristic length and S_m represents the characteristic area.

3) DERIVATION OF THREE-CHANNEL TRANSFER FUNCTION FOR THE BOOST-GLIDE ROCKET

The velocity variables are long period movements, which change slowly relative to angular variables. We usually ignore the small speed variable while designing the attitude control law. Therefore, the longitudinal perturbation model can be rewritten as

$$\begin{cases} \dfrac{d\Delta\theta}{dt} = a_{22}\Delta\theta + a_{23}\Delta\alpha + a_{25}\Delta\delta_\varphi \\ \dfrac{d\Delta\alpha}{dt} = -a_{22}\Delta\theta - a_{23}\Delta\alpha + \Delta\omega_{z1} - a_{25}\Delta\delta_\varphi \\ \dfrac{d\Delta\omega_{z1}}{dt} = a_{43}\Delta\alpha + a_{44}\Delta\omega_{z1} + a_{45}\Delta\delta_\varphi \end{cases} \tag{10}$$

The model above can be obtained by Laplace transform

$$\begin{bmatrix} s-a_{22} & -a_{23} & 0 \\ -a_{32} & s-a_{33} & -a_{34} \\ -a_{42} & -a_{43} & s-a_{44} \end{bmatrix} \cdot \begin{bmatrix} \Delta\theta(s) \\ \Delta\alpha(s) \\ \Delta\omega_{z1}(s) \end{bmatrix} = \begin{bmatrix} a_{25} \\ a_{35} \\ a_{45} \end{bmatrix} \cdot \Delta\delta_\varphi(s) \tag{11}$$

The transfer function from pitch rudder angle $\Delta\delta_\varphi(s)$ to velocity inclination angle $\Delta\theta(s)$ can be obtained as follows, (12), as shown at the bottom of the next page.

The transfer function of pitch rudder angle $\Delta\delta_\varphi(s)$ to attack angle $\Delta\alpha\,(s)$ (13), as shown at the bottom of the next page.

The transfer function from pitch rudder angle $\Delta\delta_\varphi(s)$ to pitch angle $\Delta\varphi\,(s)$ can be obtained (14), as shown at the bottom of the next page.

The lateral perturbation model is obtained by Laplace transform

$$\begin{bmatrix} s+b_{11} & b_{12} & b_{13} & b_{14} & 0 \\ 0 & s & -b_{23} & 0 & 0 \\ -b_{31} & 0 & s-b_{33} & 0 & -b_{35} \\ 0 & 0 & 0 & s & -b_{45} \\ -b_{51} & 0 & -b_{53} & 0 & s-b_{55} \end{bmatrix} \cdot \begin{bmatrix} \Delta\beta\,(s) \\ \Delta\psi\,(s) \\ \Delta\omega_{y1}\,(s) \\ \Delta\gamma\,(s) \\ \Delta\omega_{x1}\,(s) \end{bmatrix} = \begin{bmatrix} -b_{16} & 0 \\ 0 & 0 \\ b_{36} & 0 \\ 0 & 0 \\ 0 & b_{57} \end{bmatrix} \cdot \begin{bmatrix} \Delta\delta_\psi\,(s) \\ \Delta\delta_\gamma\,(s) \end{bmatrix} \tag{15}$$

The boost-glide rocket described in Fig. 1 is skid-to-turn (SST). The interaction between yaw channel and roll channel is very small by analysis of aerodynamic data. Therefore, the cross partial derivatives of yaw and roll channels can be ignored, namely

$$\begin{cases} b_{35} = \dfrac{M_{y1}^{\omega_{x1}}}{I_{y1}} \approx 0 \\ b_{51} = \dfrac{M_{x1}^{\beta}}{I_{x1}} \approx 0 \\ b_{53} = \dfrac{M_{x1}^{\omega_{y1}}}{I_{x1}} \approx 0 \end{cases} \tag{16}$$

Under action of the attitude control system, roll angle of a rocket is small, so the projection of vertical normal force of a rocket is very small so that could be ignored in the lateral side, namely

$$b_{14} \cdot \Delta\gamma = -\frac{P\sin\alpha + Y}{mV} \cdot \Delta\gamma \approx 0 \tag{17}$$

According to simplified conditions, the yaw channel model can be obtained as follows

$$\begin{bmatrix} s+b_{11} & 0 & b_{13} \\ 0 & s & -b_{23} \\ -b_{31} & 0 & s-b_{33} \end{bmatrix} \cdot \begin{bmatrix} \Delta\beta\,(s) \\ \Delta\psi\,(s) \\ \Delta\omega_{y1}\,(s) \end{bmatrix} = \begin{bmatrix} -b_{16} \\ 0 \\ b_{36} \end{bmatrix} \Delta\delta_\psi\,(s) \tag{18}$$

The roll channel model can be obtained as follows

$$\begin{bmatrix} s & -b_{45} \\ 0 & s-b_{55} \end{bmatrix} \cdot \begin{bmatrix} \Delta\gamma\,(s) \\ \Delta\omega_{x1}\,(s) \end{bmatrix} = \begin{bmatrix} 0 \\ b_{57} \end{bmatrix} \cdot \Delta\delta_\gamma\,(s) \tag{19}$$

The transfer function from yaw rudder angle $\Delta\delta_\psi\,(s)$ to yaw angle $\Delta\psi\,(s)$ can be obtained

$$\begin{aligned} G_{\Delta\delta_\psi}^{\Delta\psi}(s) &= \frac{\Delta\psi\,(s)}{\Delta\delta_\psi\,(s)} \\ &= \frac{b_{36}s + b_{11}b_{36} - b_{31}b_{16}}{s^3 + (b_{11}-b_{33})s^2 - (b_{31}+b_{11}b_{33})s} \end{aligned} \tag{20}$$

The transfer function from roll rudder angle $\Delta\delta_\gamma\,(s)$ to roll angle $\Delta\gamma\,(s)$ can be obtained

$$\begin{aligned} G_{\Delta\delta_\gamma}^{\Delta\gamma}(s) &= \frac{\Delta\gamma(s)}{\Delta\delta_\gamma(s)} = \frac{1}{s}\cdot\frac{\Delta\omega_{x1}}{\Delta\delta_\gamma(s)} = \frac{1}{s}\cdot\frac{b_{57}}{s-b_{55}} \\ &= \frac{b_{57}}{s^2 - b_{55}s} \end{aligned} \tag{21}$$

Therefore, transfer function of the three-channel for a rocket can be obtained, (22), as shown at the bottom of the next page, where the coefficient a_{ij}, b_{ij} are called dynamic coefficients calculated according to theoretical trajectory.

The transfer function of the three-channel can be rewritten as

$$\begin{cases} G_{\Delta\delta_\varphi}^{\Delta\varphi}(s) = \dfrac{n_{\varphi1}\cdot s + n_{\varphi0}}{d_{\varphi3}\cdot s^3 + d_{\varphi2}\cdot s^2 + d_{\varphi1}\cdot s + d_{\varphi0}} \\ G_{\Delta\delta_\psi}^{\Delta\psi}(s) = \dfrac{n_{\psi1}\cdot s + n_{\psi0}}{d_{\psi3}\cdot s^3 + d_{\psi2}\cdot s^2 + d_{\psi1}\cdot s} \\ G_{\Delta\delta_\gamma}^{\Delta\gamma}(s) = \dfrac{n_{\gamma0}}{d_{\gamma2}\cdot s^2 + d_{\gamma1}\cdot s} \end{cases} \tag{23}$$

where

$$\begin{cases} n_{\varphi1} = a_{45}, \quad n_{\varphi0} = a_{45}(a_{23}-a_{22}) - a_{43}a_{25} \\ d_{\varphi3} = 1, \quad d_{\varphi2} = a_{23} - a_{22} - a_{44}, \quad d_{\varphi1} \\ \qquad = a_{44}(a_{22}-a_{23}) - a_{43}, \quad d_{\varphi0} = a_{43}a_{22} \end{cases}$$

$$\begin{cases} n_{\psi1} = b_{36}, \quad n_{\psi0} = b_{11}b_{36} - b_{31}b_{16} \\ d_{\psi3} = 1, \quad d_{\psi2} = b_{11} - b_{33}, \quad d_{\psi1} = -(b_{31} + b_{11}b_{33}) \end{cases}$$

$$\begin{cases} n_{\gamma0} = b_{57} \\ d_{\gamma2} = 1, \quad d_{\gamma1} = -b_{55} \end{cases} \tag{24}$$

4) DERIVATION OF THE TRANSFER FUNCTION FOR A BOOST-GLIDE ROCKET ATTITUDE CONTROLLER

In real applications, some important problems, such as hardware limits and parameter uncertainties, are commonly seen in boost-glide rockets. Some new control methods are not suitable for practical rockets with complex flight environments. For example, the gain scheduling control method cannot ensure good global performance. For the sliding mode control method, to maintain stability, it is necessary to continuously switch control logic, which will produce chattering problems and affect the control effect. For feedback linearization method, it requires an accurate system model and all state information, which is very difficult. Then engineering applications of the feedback linearization method are limited. So an improved PID controller is adopted for the small solid-propellant boost-glide rocket. The traditional PID controller is

$$u(t) = K_p e(t) + K_i \int_0^t e(t) + K_d \frac{de(t)}{dt} \tag{25}$$

In a boost-glide rocket attitude control system, the symbol e represents attitude angle error, which is the difference between command attitude angle and actual attitude angle. The differential term is improved, angular velocity of the boost-glide rocket is direct feedback. Angular velocity is directly measured, which is easily used in the control system.

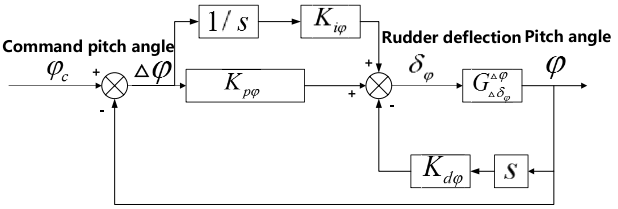

FIGURE 7. Block diagram of pitch channel control loop.

The three-channel controller can be designed as

$$\begin{aligned}
\Delta\delta_\varphi &= K_{p\varphi}\Delta\varphi + K_{i\varphi}\frac{1}{s}\Delta\varphi - K_{d\varphi}s\varphi \\
\Delta\delta_\psi &= K_{p\psi}\Delta\psi + K_{i\psi}\frac{1}{s}\Delta\psi - K_{d\psi}s\psi \\
\Delta\delta_\gamma &= K_{p\gamma}\Delta\gamma + K_{i\gamma}\frac{1}{s}\Delta\gamma - K_{d\gamma}s\gamma
\end{aligned} \tag{26}$$

5) TRANSFER FUNCTION OF THE BOOST-GLIDE ROCKET ATTITUDE CONTROL SYSTEM

Taking pitch channel as an example, the control loop is shown in Fig. 7. Yaw channel and roll channel are designed in the same method as pitch channel.

To select control parameters, the transfer function of pitch channel can be obtained. Firstly, the open-loop transfer function of pitch channel is calculated. The open-loop control block diagram is shown in Fig. 8.

$$\begin{aligned}
G^{\Delta\alpha}_{\Delta\delta_\varphi}(s) &= \frac{\Delta\alpha(s)}{\Delta\delta_\varphi(s)} \\
&= \frac{-a_{25}s^2 + (a_{44}a_{25} + a_{45})s - a_{22}a_{45}}{s^3 + (a_{23} - a_{22} - a_{44})s^2 + [a_{44}(a_{22} - a_{23}) - a_{43}]s + a_{43}a_{22}}
\end{aligned} \tag{12}$$

$$\begin{aligned}
G^{\Delta\theta}_{\Delta\delta_\varphi}(s) &= \frac{\Delta\theta(s)}{\Delta\delta_\varphi(s)} \\
&= \frac{a_{25}s^2 - a_{44}a_{25}s + a_{45}a_{23} - a_{43}a_{25}}{s^3 + (a_{23} - a_{22} - a_{44})s^2 + [a_{44}(a_{22} - a_{23}) - a_{43}]s + a_{43}a_{22}}
\end{aligned} \tag{13}$$

$$\begin{aligned}
G^{\Delta\varphi}_{\Delta\delta_\varphi}(s) &= \frac{\Delta\varphi(s)}{\Delta\delta_\varphi(s)} = \frac{\Delta\alpha(s)}{\Delta\delta_\varphi(s)} + \frac{\Delta\theta(s)}{\Delta\delta_\varphi(s)} \\
&= \frac{a_{45}s + a_{45}(a_{23} - a_{22}) - a_{43}a_{25}}{s^3 + (a_{23} - a_{22} - a_{44})s^2 + [a_{44}(a_{22} - a_{23}) - a_{43}]s + a_{43}a_{22}}
\end{aligned} \tag{14}$$

$$\begin{cases}
G^{\Delta\varphi}_{\Delta\delta_\varphi}(s) = \dfrac{a_{45}s + a_{45}(a_{23} - a_{22}) - a_{43}a_{25}}{s^3 + (a_{23} - a_{22} - a_{44})s^2 + [a_{44}(a_{22} - a_{23}) - a_{43}]s + a_{43}a_{22}} \\
G^{\Delta\psi}_{\Delta\delta_\psi}(s) = \dfrac{b_{36}s + b_{11}b_{36} - b_{31}b_{16}}{s^3 + (b_{11} - b_{33})s^2 - (b_{31} + b_{11}b_{33})s} \\
G^{\Delta\gamma}_{\Delta\delta_\gamma}(s) = \dfrac{b_{57}}{s^2 - b_{55}s}
\end{cases} \tag{22}$$

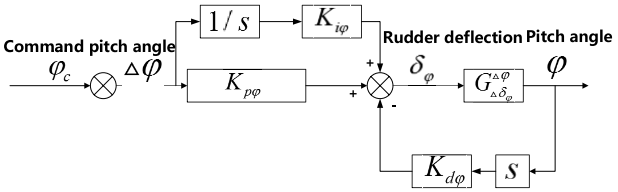

FIGURE 8. Open-loop control block diagram of pitch channel.

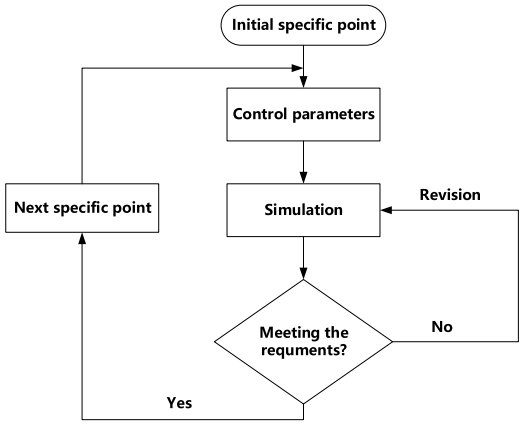

FIGURE 9. The process of control parameters correction.

According to a control block diagram in Fig. 8, the open-loop transfer function of pitch channel is

$$G^{\varphi}_{0\varphi_c}(s) = \frac{\varphi(s)}{\varphi_c(s)} = \frac{\left(K_{p\varphi} + \frac{K_{i\varphi}}{s}\right) G^{\Delta\varphi}_{\Delta\delta_\varphi}(s)}{1 + K_{d\varphi} s G^{\Delta\varphi}_{\Delta\delta_\varphi}(s)} \tag{27}$$

To select a certain moment, the transfer function of pitch channel can be calculated, (28), as shown at the bottom of the next page.

A closed-loop transfer function is calculated by the open-loop transfer function

$$G^{\varphi}_{\varphi_c}(s) = \frac{G^{\varphi}_{0\varphi_c}(s)}{1 + G^{\varphi}_{0\varphi_c}(s)} \tag{29}$$

The open-loop transfer function and closed-loop transfer function of yaw channel and roll channel can be derived same as the above method.

C. VERIFICATION PROCESS OF ATTITUDE CONTROL LAW

There are four steps to verify attitude control law.

1) SELECTION OF SPECIFIC POINTS FOR THE BOOST-GLIDE ROCKET ATTITUDE CONTROL SYSTEM

To select the specific points of flight trajectory, including engine shutdown point (maximum dynamic pressure point), highest trajectory point, pull starting point, parachute opening point, etc.

2) CALCULATION OF THE BOOST-GLIDE ROCKET THREE-CHANNEL TRANSFER FUNCTION

According to dynamic characteristics of specific points, the dynamics coefficient is calculated, then three-channel transfer function of the boost-glide rocket is obtained.

3) TO SELECT THE CONTROLLER PARAMETERS

To select the initial control parameters, $K_{p\varphi}$, $K_{i\varphi}$, $K_{d\varphi}$.

According to the open-loop transfer function, Bode diagram is drawn to calculate the frequency-domain characteristics.

According to the closed-loop transfer function, step response curve is drawn to calculate the time-domain characteristics.

To judge whether the performance indicators meet requirements. If not, adjusting the control parameters and recalculate performance indicators until performance indicators meet requirements. The control law of yaw channel and roll channel can be designed as the same method.

4) VERIFICATION AND MODIFICATION OF ATTITUDE CONTROL LAW FOR THE BOOST-GLIDE ROCKET

The control law is designed by some hypotheses, including rocket linear movement model hypothesis, no disturbance hypothesis, the ideal sensors and actuators hypothesis, etc. The actual movement model is nonlinear and time-varying, control parameters should be verified and corrected in a six-degree-freedom simulation. If the attitude diverges, we should adjust the control parameters according to simulation.

The selected control parameters of each specific point are taken as the initial value, the simulation time is set from zero to this point. The control parameters are corrected according to tracking derivation of the attitude angle along time. When attitude control correction of this specific point is finished, simulation time is extended to the next specific point. The correction process is shown in Fig. 9.

The coordination relationship of the design, verification, and modification of the boost-glide rocket control system is shown in Fig. 10.

III. NUMERICAL SIMULATION VERIFICATION

A. NUMERICAL SIMULATION VERIFICATION

The boost-glide aircraft needs to glide in the atmosphere, so a glide trajectory is designed. Designed boost-glide aircraft is recoverable with a parachute, so movement before parachute opening point is mainly simulated, and movement after parachute opening point is not the focus. For designed trajectory, the boost-glide rocket will glide in the longitudinal plane and suppresses yaw and roll movement. The designed glide trajectory in the longitudinal plane is shown in Fig. 11. Command yaw angle and command roll angle of the lateral movement is zero. It is a boost-glide trajectory so attack angle of the rocket is zero in ascending stage and changes

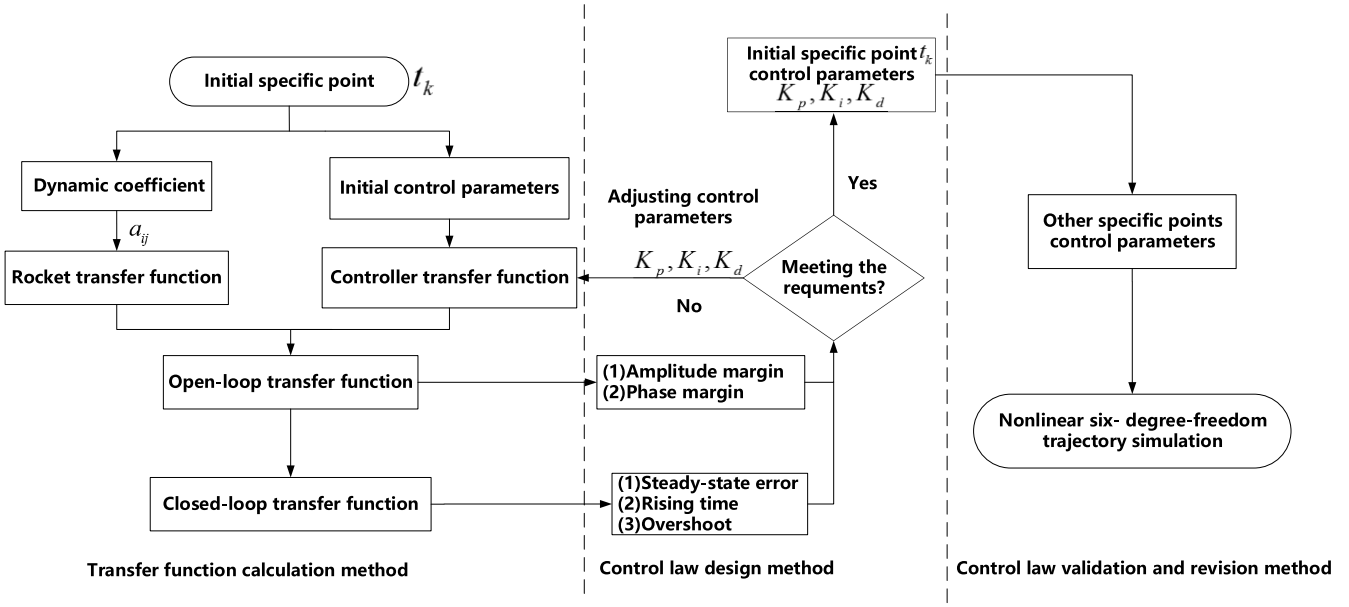

FIGURE 10. The control law design process of rocket pitch channel.

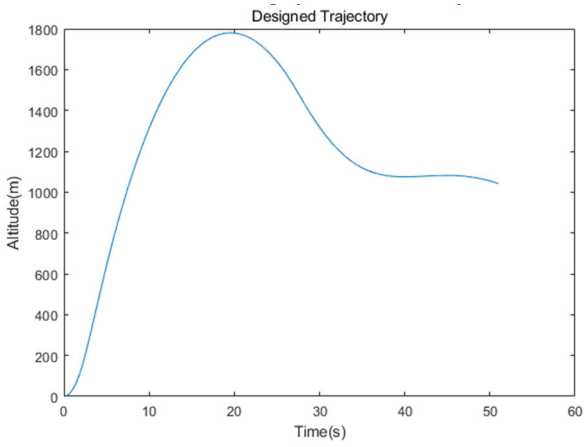

FIGURE 11. Theoretical trajectory of the boost-glide rocket.

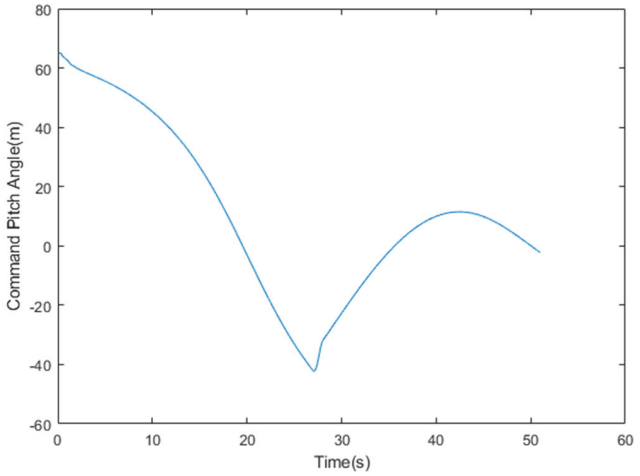

FIGURE 12. Theoretical pitch angle of the boost-glide rocket.

in descending stage with a pull-up glide trajectory to increase the range.

Design of the small boost-glide rocket does not require very strict trajectory tracking without considering the guidance problem, so it only needs to control the three-channel attitude. Theoretical trajectory of the boost-glide rocket is in the transmitting plane, therefore, command yaw angle and command roll angle of the attitude control system is zero. In order to realize the trajectory in Fig. 11, the boost-glide rocket will get lift force by adjusting pitch angle and attack angle. Then the rocket will glide in the atmosphere, theoretical pitch angle corresponding to trajectory is shown in Fig. 12. The theoretical pitch angle in Fig. 12 is as command pitch angle of the rocket, the mission is to track theoretical boost-glide trajectory. Goal of the attitude control system is to keep yaw angle and roll angle at 0, and the pitch angle needs to track command pitch angle. The rocket will realize the boost-glide trajectory with great effect by tracking command attitude angle.

$$G^{\varphi}_{0\varphi_c}(s) = \frac{K_{p\varphi} \cdot n_{\varphi 1} \cdot s^2 + \left(K_{p\varphi} \cdot n_{\varphi 0} + K_{i\varphi} \cdot n_{\varphi 1}\right) \cdot s + K_{i\varphi} \cdot n_{\varphi 0}}{d_{\varphi 3} \cdot s^4 + \left(d_{\varphi 2} + K_{d\varphi} \cdot n_{\varphi 1}\right) \cdot s^3 + \left(d_{\varphi 1} + K_{d\varphi} \cdot n_{\varphi 0}\right) \cdot s^2 + d_{\varphi 0} \cdot s} \tag{28}$$

TABLE 1. Selection of specific points.

The time of specific points	Meaning
0.5s	near control starting point
2s	assistant point
3.8s	near maximum dynamic pressure point
18.45	near highest trajectory point
27	near pull starting point
52	near parachute opening point

B. SPECIFIC POINTS SELECTION FOR THE BOOST-GLIDE ROCKET ATTITUDE CONTROL SYSTEM

Design of control law based on three-channel transfer function of the boost-glide rocket is aimed at a certain moment in the flight trajectory. If the whole flight process should be controlled stably, the representative moment in flight trajectory should be selected.

The small boost-glide experimental rocket should have the function of full rocket recovery to analyze the flight process efficiently. According to parachute opening time, movement of the boost-glide rocket before parachute opening point is mainly simulated, and movement after parachute opening point is not the focus. The control starting point, maximum dynamic pressure point, highest trajectory point, pull starting point and parachute opening point are selected here. To ensure coordination of the whole rocket movement, another specific point is taken between the starting point and the engine shutdown point, so 6 specific points are selected in total. The time of each specific point is determined according to the theoretical trajectory as shown in Table 1.

In table 1, the boost-glide rocket has maximum speed and maximum dynamic pressure at engine shutdown point, and pull starting point is the moment while the boost-glide rocket starts to pull up. The parachute opening point is the moment while attitude of the boost-glide rocket is near 0 in descending stage. The control parameters corresponding to time between each specific point are obtained by linear interpolation of specific points.

C. CONTROL LAW VERIFICATION

The performance indicators of attitude control system:

1) The amplitude margin is greater than 10dB.
2) The phase margin is greater than 45°.
3) Overshoot is less than 15%.
4) Rising time is less than 3 seconds.
5) Steady-state error is less than 0.01.

The boost-glide rocket needs to glide in the atmosphere by changing attack angle and attitude angle. The moment of pull starting point is valuable, which faces great difficulties in the attitude control system.

Taking pitch channel attitude control law design of pull starting point as an example to analyze. Design of the three-channel attitude control system at other specific points is similar to pitch channel at pull starting point.

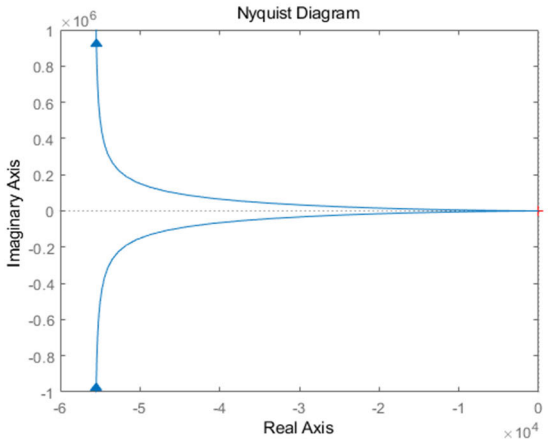

FIGURE 13. Nyquist diagram of pitch channel.

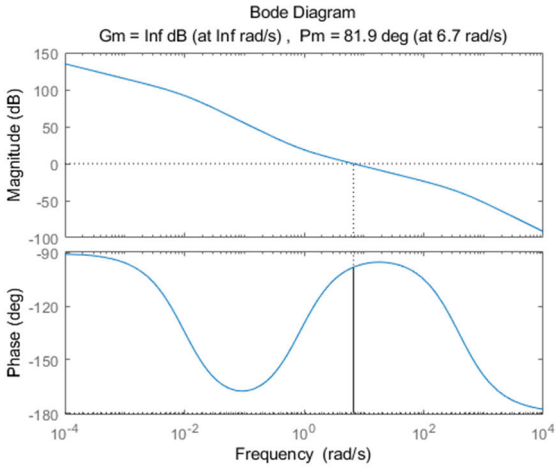

FIGURE 14. Bode diagram of pitch channel.

According to the attitude control law design method proposed above, the time of engine ignition is regarded as zero point. The time of pull starting point is 27s, the transfer function of pitch channel can be obtained as follows

$$G_{\Delta\delta_0}^{\Delta\varphi}(s) = \frac{-2.6636s - 2.9725}{s^3 + 2.2483s^2 + 59.4734s + 3.4251} \tag{30}$$

where $K_{p\varphi} = -20, K_{i\varphi} = -20, K_{d\varphi} = -3$, the open-loop transfer function of pitch channel is

$$G_{0\varphi_c}^{\varphi}(s) = \frac{3052.2608s^2 + 6458.4949s + 3406.2341}{s^4 + 460.0874s^3 + 570.4085s^2 + 3.4251s} \tag{31}$$

The closed-loop transfer function of pitch channel is (32), as shown at the bottom of the next page.

Nyquist diagram, Bode diagram, and step response curve according to transfer function above are shown in Fig. 13-Fig. 15. Performance indicators according to the transfer function above are shown in Table 2. PID parameters selected of other specific points are shown in Table3. Selection of PID parameters should ensure attitude angle does not diverge with time and performance indicators are supposed

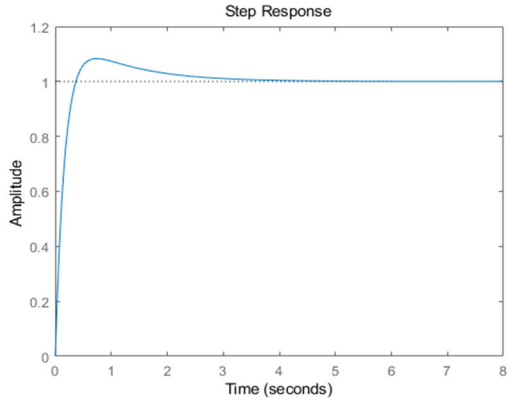

FIGURE 15. Step response curve of pitch channel.

TABLE 2. Performance indicators of pitch channel at pull starting point.

Names of indicators	Magnitude	Whether meeting requirements
amplitude margin Gm	inf dB	√
phase margin Pm	81.9082 °	√
overshoot σ%	8.3153%	√
rising time tr	0.25068 s	√
steady-state error ess	0	√
open-loop poles	s=0, -388.7166, -0.9944, -0.01	√
closed-loop poles	s=-381.9629, -5.7719, -1.0282, -0.9579	√

TABLE 3. PID parameters of each specific point.

Channels	Courses	Time(s) [0.5 2 3.8 18.45 27 52]
roll channel	P	[1 1 1 1 2 2]*(-1)
	I	[1 2 2 1 1 1]* (-1)
	D	[0.1 0.2 0.2 0.1 0.5 0.5]* (-1)
yaw channel	P	[1 0 2 2 3 5]* (-1)
	I	[10 15 25 5 1 1]* (-1)
	D	[0.1 0.2 0.2 2 3 2]* (-1)
pitch channel	P	[1 2 5 10 20 10]* (-1)
	I	[1 1 1 2 2 2.5]* (-10)
	D	[0.3 0.3 0.2 0.5 3 1.5]* (-1)

to be as optimal as possible for practical boost-glide rocket systems.

D. ANALYSIS OF SIMULATION RESULTS

Designed parachute opening time is 51s after engine ignition, then the boost-glide rocket falls free for recovery. It is enough to ensure that the control system works to the parachute opening time. So the moving process from engine ignition to parachute opening is simulated.

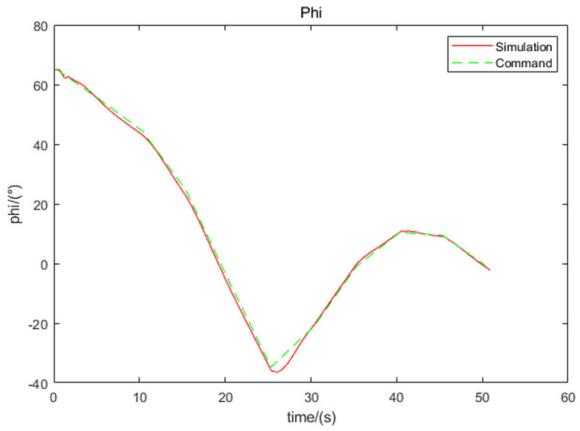

FIGURE 16. Comparison between simulation value and command value of pitch angle curve.

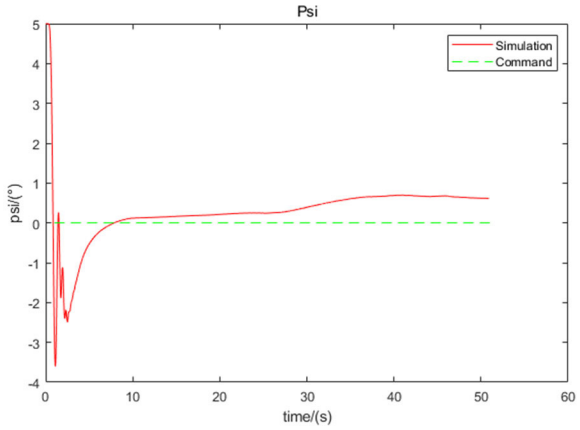

FIGURE 17. Comparison between simulation value and command value of yaw angle curve.

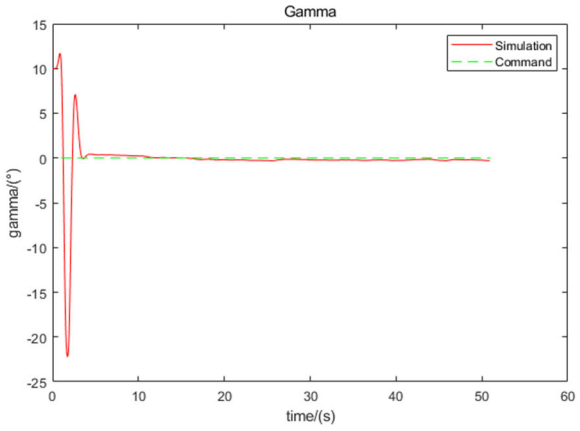

FIGURE 18. Comparison between simulation value and command value of roll angle curve.

$$G_{\varphi_c}^{\varphi}(s) = \frac{3052.2608s^2 + 6458.4949s + 3406.2341}{s^4 + 460.0874s^3 + 3622.6693s^2 + 6461.92s + 3406.2341} \tag{32}$$

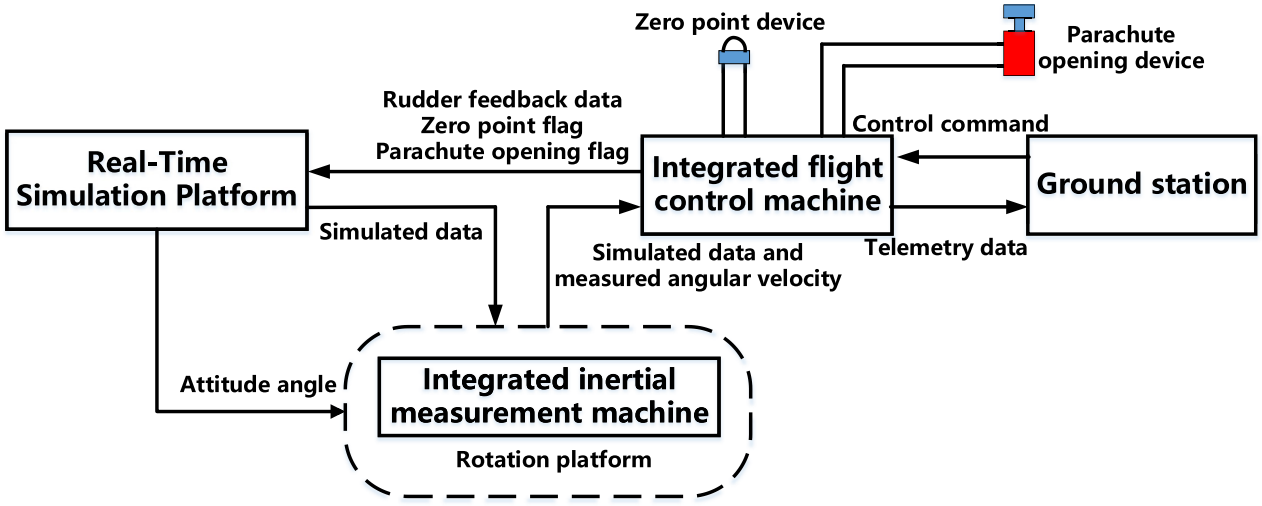

FIGURE 19. Schematic diagram of hardware-in-the-loop simulation.

It is assumed that the boost-glide rocket is launched with initial angle and the initial pitch angle is set as 65°, the initial yaw angle is set as 5°, and the initial roll angle is set as 10 °, to verify the control effect of the designed attitude control system.

A six-degree-freedom model of rocket is established in Real-Time Simulation Platform, designed trajectory is discretized according to specific points, then the linear interpolation method is used to calculate the command attitude angle. The selected PID control parameters at each specific point are brought into the six-degree-freedom model of rocket to obtain simulation results, as shown in Fig. 16- Fig. 18.

In Fig. 16- Fig. 18, the x-coordinate is time, the y-coordinate is attitude angle, phi represents pitch angle, psi represents yaw angle, and gamma represents roll angle. Command represents command attitude angle, Simulation represents simulation attitude angle.

We can conclude that selected PID control parameters of specific points have a good control effect according to simulation. The simulation value and the command value are coincide basically. In the case of a large initial error of yaw angle and roll angle, it can quickly converge and track the command attitude angle. It is proved that design method of the attitude control system is reasonable and ideal control effect can be achieved.

IV. HARDWARE-IN-THE-LOOP SIMULATION VERIFICATION

Real-Time Simulation Platform, integrated flight control machine, integrated inertial measurement machine, ground station, rotation platform and other hardware are used for closed-loop hardware-in-the-loop simulation according to the schematic diagram shown in Fig. 19.

Real-Time Simulation Platform uses the rudder deflection angle calculated by integrated flight control machine to finish closed-loop trajectory simulation, which drives rotation

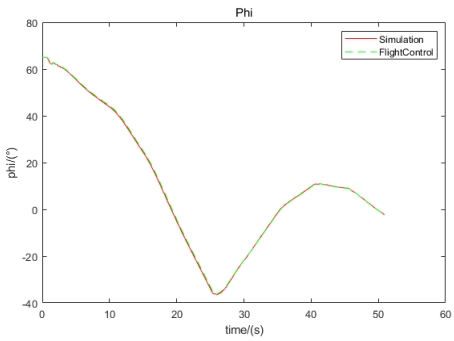

FIGURE 20. Comparison between simulated values and experimental values of pitch angle curve.

platform to simulate rocket flight attitude. The simulated flight data is transmitted to integrated inertial measurement machine, then the mixed data with simulated data and measured angular velocity data is transmitted to integrated flight control machine to complete guidance, navigation, and control calculation.

The simulation results of Real-Time Simulation Platform are used as standard values to verify the hardware-in-the-loop simulation control effect, as shown in Fig. 20- Fig. 23.

In Fig. 20- Fig. 22, the x-coordinate is time, the y-coordinate is attitude angle, phi represents pitch angle, psi represents yaw angle, and gamma represents roll angle. Simulation represents simulated attitude angle of Real-Time Simulation Platform. FlightControl represents experimental attitude angle of the hardware-in-the-loop simulation experiment. In Fig. 23, the x-coordinate is time, the y-coordinate is deviation of attitude angle.

To calculate the mean and standard deviation of error for hardware-in-the-loop simulation, as shown in Table 4.

It can be seen from Fig. 20- Fig. 23 that the numerical simulation value is regarded as the ideal control effect, and

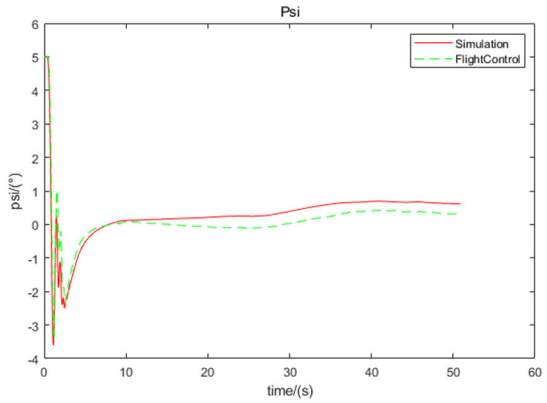

FIGURE 21. Comparison between simulated values and experimental values of yaw angle curve.

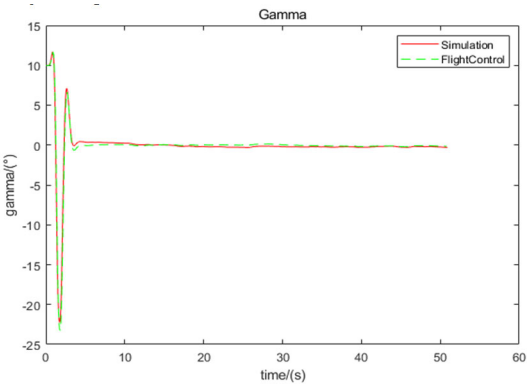

FIGURE 22. Comparison between simulated values and experimental values of roll angle curve.

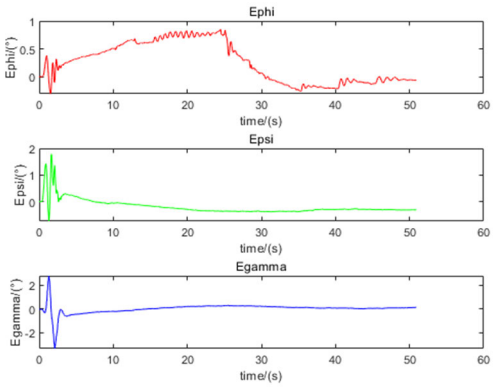

FIGURE 23. Deviation curve between simulated attitude angle and experimental attitude angle.

the hardware-in-the-loop simulation value is regarded as the actual control effect. The deviation of pitch angle is kept within 1°, and the deviation of yaw angle and roll angle converges quickly and approaches zero. The control effect is good and desired effect is achieved. It is proved that design method of the attitude control system for a small solid-propellant boost-glide rocket is feasible and the control effect is good.

TABLE 4. The mean and standard deviation of error for hardware-in-the-loop simulation.

Attitude angle	Mean of the error(°)	Standard deviation of the error(°)
pitch angle	0.2513	0.3560
yaw angle	-0.1836	0.2731
roll angle	0.0345	0.4101

V. CONCLUSION

Design method of the attitude control system is proposed based on a dynamic model of a small solid-propellant boost-glide rocket. An improved PID controller is used to design the attitude control law, and designed attitude control law is brought into a six-degree-freedom model of the boost-glide rocket for verification. The hardware-in-the-loop simulation experiment scheme is proposed, and hardware of the small solid-propellant boost-glide rocket is connected to a closed-loop experiment to simulate the real flight environment. Experimental results show that attitude deviation converges quickly and the control effect is great. Proposed analysis method and design process can be applied for practical boost-glide rocket systems in the future.

REFERENCES

[1] I.-S. Jeon, J.-I. Lee, and M.-J. Tahk, "Homing guidance law for cooperative attack of multiple missiles," *J. Guid., Control, Dyn.*, vol. 33, no. 1, pp. 275–280, 2010.
[2] J. Zeng, L. Dou, and B. Xin, "A joint mid-course and terminal course cooperative guidance law for multi-missile salvo attack," *Chin. J. Aeronaut.*, vol. 31, no. 6, pp. 1311–1326, Jun. 2018.
[3] M. Chen, G. Tao, and B. Jiang, "Dynamic surface control using neural networks for a class of uncertain nonlinear systems with input saturation," *IEEE Trans. Neural Netw. Learn. Syst.*, vol. 26, no. 9, pp. 2086–2097, Sep. 2015.
[4] H.-J. Uang and B.-S. Chen, "Robust adaptive optimal tracking design for uncertain missile systems: A fuzzy approach," *Fuzzy Sets Syst.*, vol. 126, no. 1, pp. 63–87, Feb. 2002.
[5] S.-H. Kim, Y.-S. Kim, and C. Song, "A robust adaptive nonlinear control approach to missile autopilot design," *Control Eng. Pract.*, vol. 12, no. 2, pp. 149–154, Feb. 2004.
[6] M. Hou, X. Liang, and G. Duan, "Adaptive block dynamic surface control for integrated missile guidance and autopilot," *Chin. J. Aeronaut.*, vol. 26, no. 3, pp. 741–750, 2013.
[7] X. Lidan, Z. Ke'nan, C. Wanchun, and Y. Xingliang, "Optimal control and output feedback considerations for missile with blended aero-fin and lateral impulsive thrust," *Chin. J. Aeronaut.*, vol. 23, no. 4, pp. 401–408, Aug. 2010.
[8] G. Yuan and X. Shi, "Nonlinear adaptive controller design for missile system with special uncertainties," (in Chinese), *Elect. Mach. Control*, vol. 14, no. 5, pp. 104–108, 2010.
[9] Y. Zhang, Z. Li, Z. Cheng, L. Liu, and Y. Wang, "Attitude tracking control reconfiguration for space launch vehicle with thrust loss fault," *IEEE Access*, vol. 7, pp. 184353–184364, 2019, doi: 10.1109/ACCESS.2019.2959836.
[10] Q. Shen, C. Yue, C. H. Goh, and D. Wang, "Active fault-tolerant control system design for spacecraft attitude maneuvers with actuator saturation and faults," *IEEE Trans. Ind. Electron.*, vol. 66, no. 5, pp. 3763–3772, May 2019.
[11] Z. Gao, B. Jiang, P. Shi, J. Liu, and Y. Xu, "Active fault-tolerant tracking control for near-space vehicle attitude dynamics with actuator faults," *Proc. Inst. Mech. Eng., I, J. Syst. Control Eng.*, vol. 225, no. 3, pp. 413–422, May 2011.
[12] Q. Yang, S. S. Ge, and Y. Sun, "Adaptive actuator fault tolerant control for uncertain nonlinear systems with multiple actuators," *Automatica*, vol. 60, pp. 92–99, Oct. 2015.

[13] T. A. Johansen and T. I. Fossen, "Control allocation—A survey," *Automatica*, vol. 49, no. 5, pp. 1087–1103, 2013.
[14] M. E. N. Sørensen, S. Hansen, M. Breivik, and M. Blanke, "Performance comparison of controllers with fault-dependent control allocation for UAVs," *J. Intell. Robotic Syst.*, vol. 87, no. 1, pp. 187–207, Jul. 2017.
[15] Q. Shen, D. Wang, S. Zhu, and E. K. Poh, "Control allocation based fault-tolerant control design for spacecraft attitude tracking," in *Proc. 53rd IEEE Conf. Decis. Control*, Dec. 2014, pp. 4983–4988.
[16] Y. Zhang, S. Tang, and J. Guo, "Adaptive-gain fast super-twisting sliding mode fault tolerant control for a reusable launch vehicle in reentry phase," *ISA Trans.*, vol. 71, pp. 380–390, Nov. 2017.
[17] C. Jing, H. Xu, X. Niu, and X. Song, "Adaptive nonsingular terminal sliding mode control for attitude tracking of spacecraft with actuator faults," *IEEE Access*, vol. 7, pp. 31485–31493, 2019.
[18] X. Yin, B. Wang, L. Liu, and Y. Wang, "Disturbance observer-based gain adaptation high-order sliding mode control of hypersonic vehicles," *Aerosp. Sci. Technol.*, vol. 89, pp. 19–30, Jun. 2019.
[19] B. Jung, Y. Kim, and C. Ha, "Fault tolerant fight control system design using a multiple model adaptive controller," *Proc. Inst. Mech. Eng., G, J. Aerosp. Eng.*, vol. 223, no. 1, pp. 39–50, 2009.
[20] B. Jung, S.-K. Jeong, D.-H. Lee, and Y. Kim, "Adaptive reconfigurable fight control system using multiple model mode switching," *IFAC Proc.*, vol. 38, no. 1, pp. 115–120, 2005.
[21] M. Rodrigues, D. Theilliol, and D. Sauter, "Fault tolerant control design for switched systems," *Anal. Des. Hybrid Syst.*, vol. 39, no. 5, pp. 223–228, 2006.
[22] X. Lv, B. Jiang, R. Qi, and J. Zhao, "Survey on nonlinear reconfigurable fight control," *J. Syst. Eng. Electron.*, vol. 24, no. 6, pp. 971–983, Dec. 2013.
[23] C. Wei, Y. Shen, X. Ma, X. Ma, J. Guo, and N. Cui, "Optimal formation keeping control in missile cooperative engagement," *Aircr. Eng. Aerosp. Technol.*, vol. 84, no. 6, pp. 376–389, Oct. 2012.
[24] C. Wei, J. Guo, B. Lu, Y. Shen, and L. Zhang, "Adaptive control for missile formation keeping under leader information unavailability," in *Proc. 10th IEEE Int. Conf. Control Autom. (ICCA)*, Jun. 2013, pp. 902–907.
[25] X. Wang, H. Fang, L. Dou, B. Xin, and J. Chen, "Integrated distributed formation flight control with aerodynamic constraints on attitude and control surfaces," *Nonlinear Dyn.*, vol. 91, no. 4, pp. 2331–2345, Mar. 2018.
[26] K. J. Chen, L. H. Liu, and Y. H. Meng, "Flight dynamics and guidance of long range rockets," in *Proc. NDIP*, Beijing, China, 2013, pp. 66–89.

XIAOSHUAI FAN received the B.E. degree from the College of Mechanical Engineering, Changchun University of Science and Technology. He is currently pursuing the M.E. degree with the College of Aerospace and Engineering, National University of Defense Technology. His research interests include guidance, navigation, and control of missiles.

XIBIN BAI received the B.S. degree in space engineering and the M.S. and Ph.D. degrees from the College of Aerospace and Engineering, National University of Defense Technology, Changsha, China, in 2011, 2013, and 2018, respectively. Since 2019, he has been a Lecturer with the National University of Defense Technology. His research interests include inertial navigation and aircraft dynamics and control.

ZHENYU JIANG received the B.S. degree in space engineering and the M.S. and Ph.D. degrees from the College of Aerospace and Engineering, National University of Defense Technology, Changsha, China. He has been a Professor with the National University of Defense Technology. His research interest includes aircraft overall design.

LONGBIN LIU received the Ph.D. degree in aircraft design from Beihang University, Beijing, China. He is currently an Associate Professor with the National University of Defense Technology. His research interests include aircraft conceptual design and missile structure-related areas.

SHIFENG ZHANG received the B.E., M.E., and Ph.D. degrees from the College of Aerospace Science and Engineering, National University of Defense Technology. He is currently a Professor with the College of Aerospace Science and Engineering, National University of Defense Technology. His research interest includes active disturbance rejection control of aircraft.